Supplement of Atmos. Chem. Phys., 22, 805–821, 2022
https://doi.org/10.5194/acp-22-805-2022-supplement

Atmospheric Chemistry and Physics Open Access

Supplement of

Field observational constraints on the controllers in glyoxal (CHOCHO) reactive uptake to aerosol

Dongwook Kim et al.

Correspondence to: Kyung-Eun Min (kemin@gist.ac.kr)

S1. Model input data range and treatment

Table S1. List of NASA DC-8 research flights, date of take-off based on UTC. The research flights, 01 and 03 were not included in this study due to unavailability of glyoxal (CHOCHO) data.

Research Flight Number	Date of Take-off	Inclusion in this study
01	01/May/2016	No
02	03/May/2016	Yes
03	04/May/2016	No
04	06/May/2016	Yes
05	10/May/2016	Yes
06	11/May/2016	Yes
07	12/May/2016	Yes
08	16/May/2016	Yes
09	17/May/2016	Yes
10	19/May/2016	Yes
11	21/May/2016	Yes
12	24/May/2016	Yes
13	26/May/2016	Yes
14	29/May/2016	Yes
15	30/May/2016	Yes
16	01/June/2016	Yes
17	02/June/2016	Yes
18	04/June/2016	Yes
19	08/June/2016	Yes
20	09/June/2016	Yes

S2. Data preparation; pseudo-1-minute VOC data and aerosol surface area density (A_{surf})

For constraining our 0-D box model F0AM (Framework for 0-Dimensional Atmospheric Modeling), with VOCs (Volatile Organic Compounds) measurements in lower time resolution than 1 minute, (i.e., species from WAS, Whole Air Samples, Simpson et al. 2020), "pseudo" 1-minute interpolation scheme, which is similar to Schroeder et al. (2020), was used based on the relation between co-varying VOCs species. The main difference is that Schroeder et al. derived 1 second VOCs data from WAS while we only used this scheme to interpolate 1-minute data where the observations are missing, mainly in between sample canisters.

For the species where high time resolution measurements are available (e.g., ethane, propane, toluene, and benzene, etc.) from either PTR-ToF-MS (Proton Transfer Reaction Time of Flight Mass Spectrometer) or CAMS (Compact Atmospheric Multi-Species Spectrometer), the averaged ratio of WAS VOCs and those from PTR-ToF-MS or CAMS for 31 consecutive data points (15 points before and after) were used to interpolate the missing data in WAS in 1-minute time resolution. Once the pseudo-1minute interpolated data were prepared for these species, we allow them as reference species to maximize the covariance with the target species to reflect the varying source signatures among different air masses. Reference species were determined by the best correlation with the target species as listed in Table S2. Figure S1 shows an example time series of 4 individual chemicals (e.g., toluene, m/p-xylenes, ethene and isoprene) from original WAS (orange circles) and interpolated pseudo-1-minute data (blue lines) together with reference data (gray dots) during the RF (Research Flight) 17.

Total aerosol surface area density (A_{surf}) was calculated from the dry aerosol number distribution from SMPS (Scanning Mobility Particle Sizer) and LAS (Laser Aerosol Spectrometer) in the size range of 10 nm to 1.2 μm. For LAS, the measured optical diameter, based on PSL (PolyStyrene Latex) calibration was corrected by multiplying 1.115 to account for the differences in refractive indices of PLS and ambient aerosols. (Nault et al., 2018) Also, Also, the aerosol number concentration from LAS had been corrected by 1.56 to reflect the underestimation in LAS volume against black carbon included AMS volume mainly owing to the saturation effects in the measurements. (Nault et al., 2018)

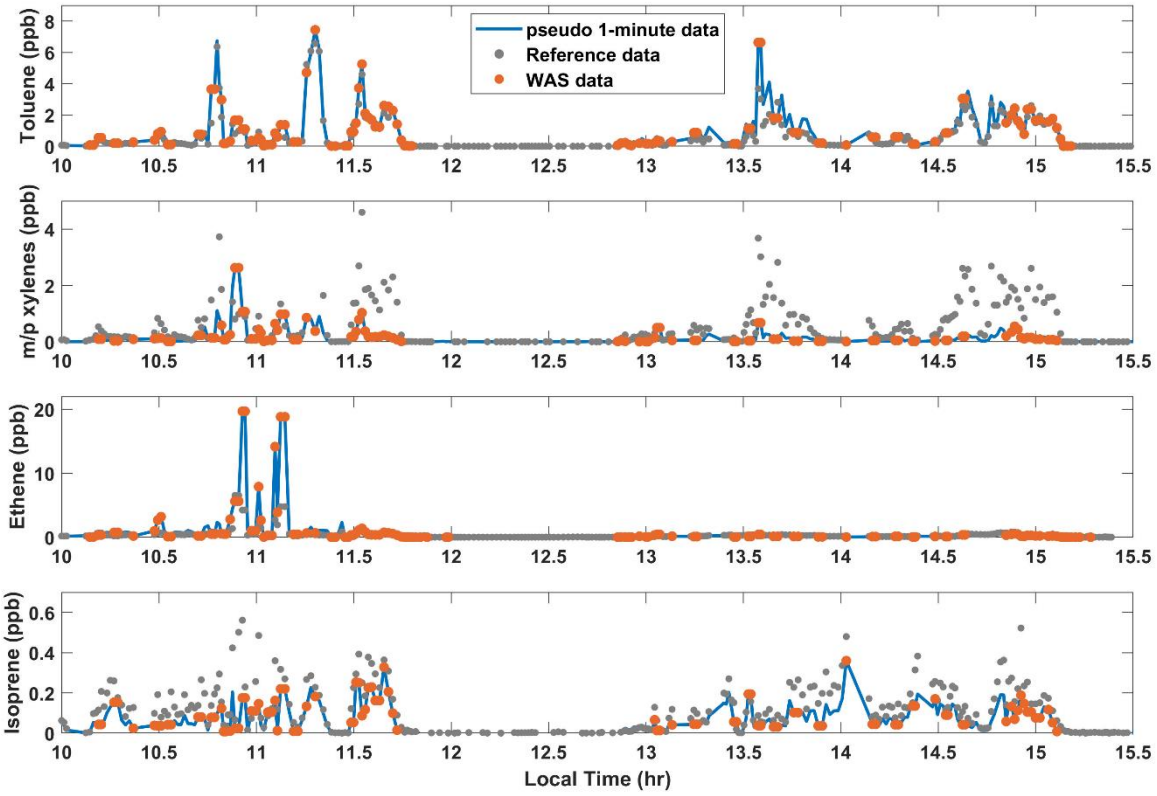

Figure S1. An example time series of interpolated pseudo-1-minute data (blue lines) and WAS data (orange circles) together with reference data (gray dots) during RF 17. Toluene, m/p xylenes, ethene and isoprene are shown from the top to the bottom.

Table S2. 0-D box model constrained species information. The reference VOCs column represents the remarked species for pseudo-1-minute data interpolation. Background concentrations were treated as 0 unless specified.

Class	Species or Parameter	Instrument Name	Reference VOC species
Inorganic	Methane	TDLAS	-
	Carbon monoxide	TDLAS	-
	Nitrogen dioxide	Chemiluminescence	-
	Sulfur dioxide	GIT-CIMS	
Alkanes	n-Ethane	WAS	Ethane (CAMS)
	n-Propane	WAS	Ethane (CAMS)
	Isobutane	WAS	n-Propane (pseudo-1min.)
	n-Butane	WAS	Isobutene (pseudo-1min.)
	Isopentane	WAS	n-Butane (pseudo-1min.)
	n-Pentane	WAS	Isopentane (pseudo-1min.)
	Cyclohexane	WAS	Toluene (pseudo-1min.)
	n-Hexane	WAS	n-Propane (pseudo-1min.)
	2,3-Dimethylbutane	WAS	Hexane (pseudo-1min.)
	2-Methylpentane	WAS	2,3-Dimethylbutane (pseudo-1min.)
	3-Methylpentane	WAS	2-Methylpentane (pseudo-1min.)
	n-Heptane	WAS	n-Butane (pseudo-1min.)
	n-Octane	WAS	n-Butane (pseudo-1min.)
	n-Nonane	WAS	n-Octane (pseudo-1min.)
	n-Decane	WAS	n-Nonane (pseudo-1min.)
Alkenes	Ethene	WAS	n-Butane (pseudo-1min.)
	Propene	WAS	Ethene (pseudo-1min.)

	1-Butene	WAS	Propene (pseudo-1min.)
	Isobutene	WAS	1-Butene (pseudo-1min.)
	trans-2-Butene	WAS	Isobutene (pseudo-1min.)
	cis-2-Butene	WAS	trans-2-Butene (pseudo-1min.)
	1,3-Butadiene	WAS	Propene (pseudo-1min.)
Alkynes	Ethyne	WAS	Benzene (PTR-TOF-MS)
Aromatics	Benzene	WAS	Benzene (PTR-TOF-MS)
	Toluene	WAS	Toluene (PTR-TOF-MS)
	m,p-Xylene	WAS	Toluene (PTR-TOF-MS)
	o-Xylene	WAS	Toluene (PTR-TOF-MS)
	Ethylbenzene	WAS	C8 alkylbenzenes (PTR-TOF-MS)
	3-Ethyltoluene	WAS	C8 alkylbenzenes (PTR-TOF-MS)
	2-Ethyltoluene	WAS	3-Ethyltoluene (pseudo-1min.)
	4-Ethyltoluene	WAS	3-Ethyltoluene (pseudo-1min.)
	1,2,4-Trimethylbenzene	WAS	3-Ethyltoluene (pseudo-1min.)
	1,2,3-Trimethylbenzene	WAS	1,2,4-Trimethylbenzene (pseudo-1min.)
	1,3,5-Trimethylbenzene	WAS	1,2,3-Trimethylbenzene (pseudo-1min.)
	n-Propylbenzene	WAS	C8 alkylbenzenes (PTR-TOF-MS)
	Isopropylbenzene	WAS	n-Propylbenzene (pseudo-1min.)
Biogenic VOCs	Isoprene	WAS	Isoprene (PTR-TOF-MS)
	alpha-Pinene	WAS	Monoterpenes (PTR-TOF-MS)
	beta-Pinene	WAS	Monoterpenes (PTR-TOF-MS)
Meteorology	Temperature, K	DC8-Hsking	-
	Pressure, hPa	DC8-Hsking	-

Relative Humidity, %	DLH	-
Photolysis Frequencies, /s	CAFS	-
Ozone Column, DU	4STAR[a]	-

[a]Sperctrometer for Sky-Scanning, Sun-Tracking Atmospheric Research (4STAR)

S3. Photochemical age dependency treatment.

Our model assumes a full-day evolution for oxygenated VOCs (oVOCs) estimation to account for the contribution from unmeasured intermediates in VOC oxidation paths. This is a legitimate approach especially for box modeling works with airborne measurements (Marvin et al. 2017; Brune et al. 2020), however, air mass age dependent bias cannot be ruled out. F0AM with a full day evolution likely overestimates oVOCs for the fresh plumes near source regions than reality, since this air mass tends to have not enough time for oxidation products to build up. On the other hand, aged plumes are likely to be over-processed than just a day, thus our model tends to underestimate such cases. As shown in Fig. S2a, F0AM underestimates HCHO when $Photo_{age}$ (photochemical age defined by NO_x/NO_y as described in section 2.3 in the main text) is high. In this case, for calculation of $Photo_{age}$, OH concentration of 1.5×10^6 molecules cm^{-3} was used to calculate photochemical age as other previous studies (DeCarlo et al., 2010; Hayes et al., 2013; Freney et al., 2014; Hu et al., 2016; Ortega et al., 2016; Ma et al., 2017; Nault et al., 2018) to compare with preceding works. Due to this limitation in our diurnal steady-state box model, photochemical age dependent bimodal relations in modeled to observed HCHO concentrations were found in Fig. S2c.

A photochemical age dependent adjustment was introduced for the production rates in CHOCHO based on the relationship between the ratio of modeled and measured HCHO against $Photo_{age}$ (Fig. S2a). The mean percent difference in measured and modeled HCHO changes from -12.5 ($\pm$41.5 %) to 1.92 ($\pm$39.4 %). Also, the possible difference in effective uptake rate coefficient of CHOCHO ($k_{eff,uptake}$) owing to this adjustment is 27 % as described in Fig. S3.

One should note that this adjustment was not for the better agreement in modeled to observed HCHO (Fig. S2c-d) but for the process age dependency; as shown in Fig. S2c-d, measured and modeled HCHO agreement without (without) this adjustment shows high (low) correlation slope as 1.08 (1.23) than the other case. Similar effects were also found for other oVOCs, and here we only show OH reactivity (OHR) as a representative of the whole oVOCs.

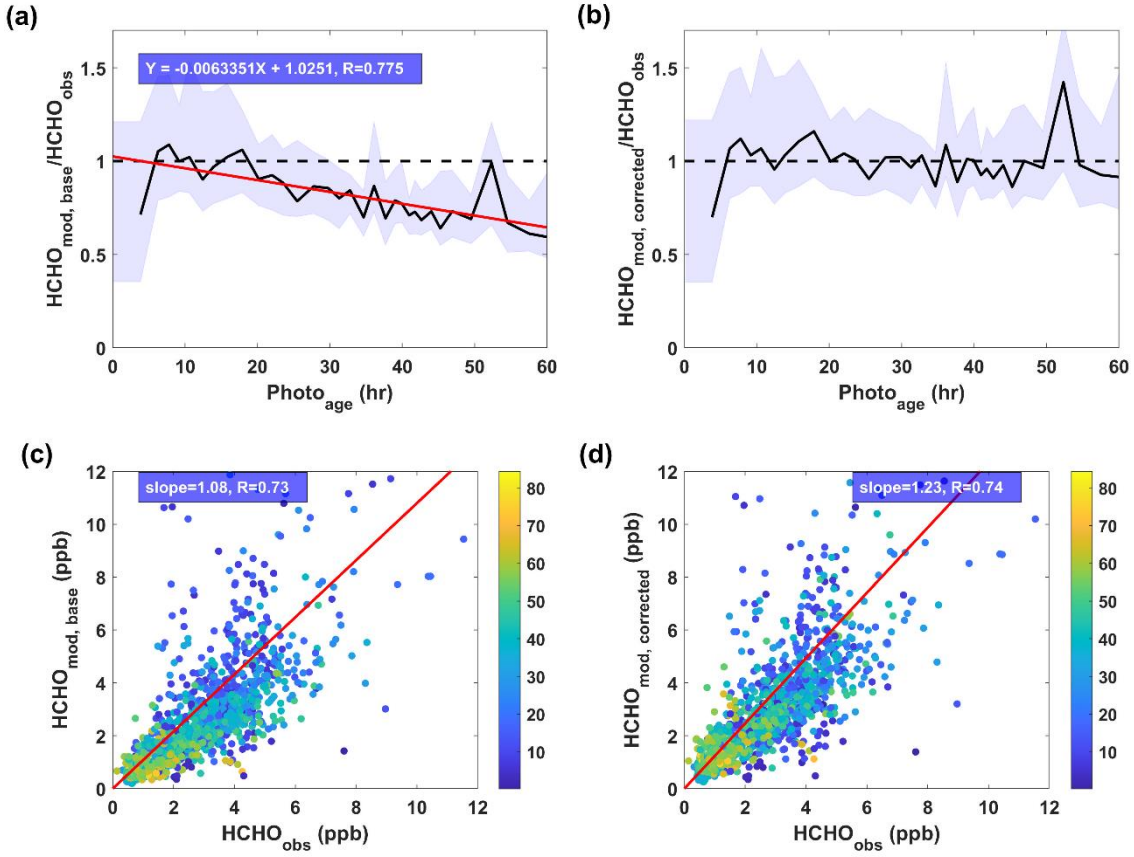

Figure S2. Photochemical age (*Photo*$_{age}$) dependence in modeled to measured HCHO ratio for (a) before and (b) after the *Photo*$_{age}$ adjustment. And 1:1 plot of measured to modeled HCHO (c) before and (d) after that adjustment where the color bars represent the *Photo*$_{age}$ (hr) calculated assuming OH=1.5x10^{5} molecule cm^{-3}. Black lines in (a) and (b) show the median and blue shades are the interquartile range. Regression lines in red on (c) and (d) are least-orthogonal-distance regression (ODR) forced through zero intercept.

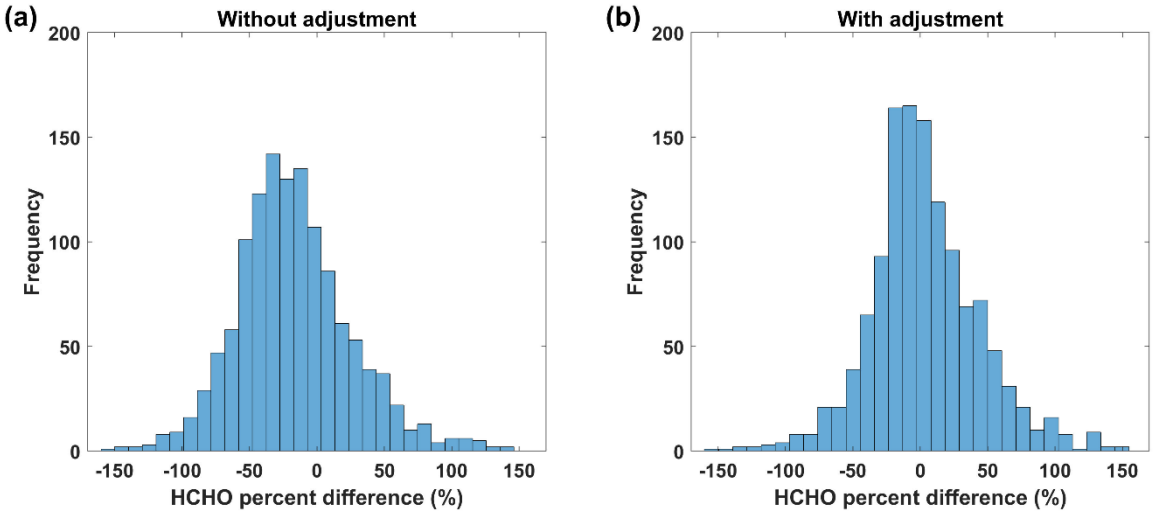

Figure S3. The percent difference between modeled and measured HCHO (a) before and (b) after the $Photo_{age}$ bias adjustment. The mean percent difference is -12.52 ± 41.46 % (± 1σ) and 1.92 ± 39.40 % (± 1σ) for HCHO without and with adjustment, respectively.

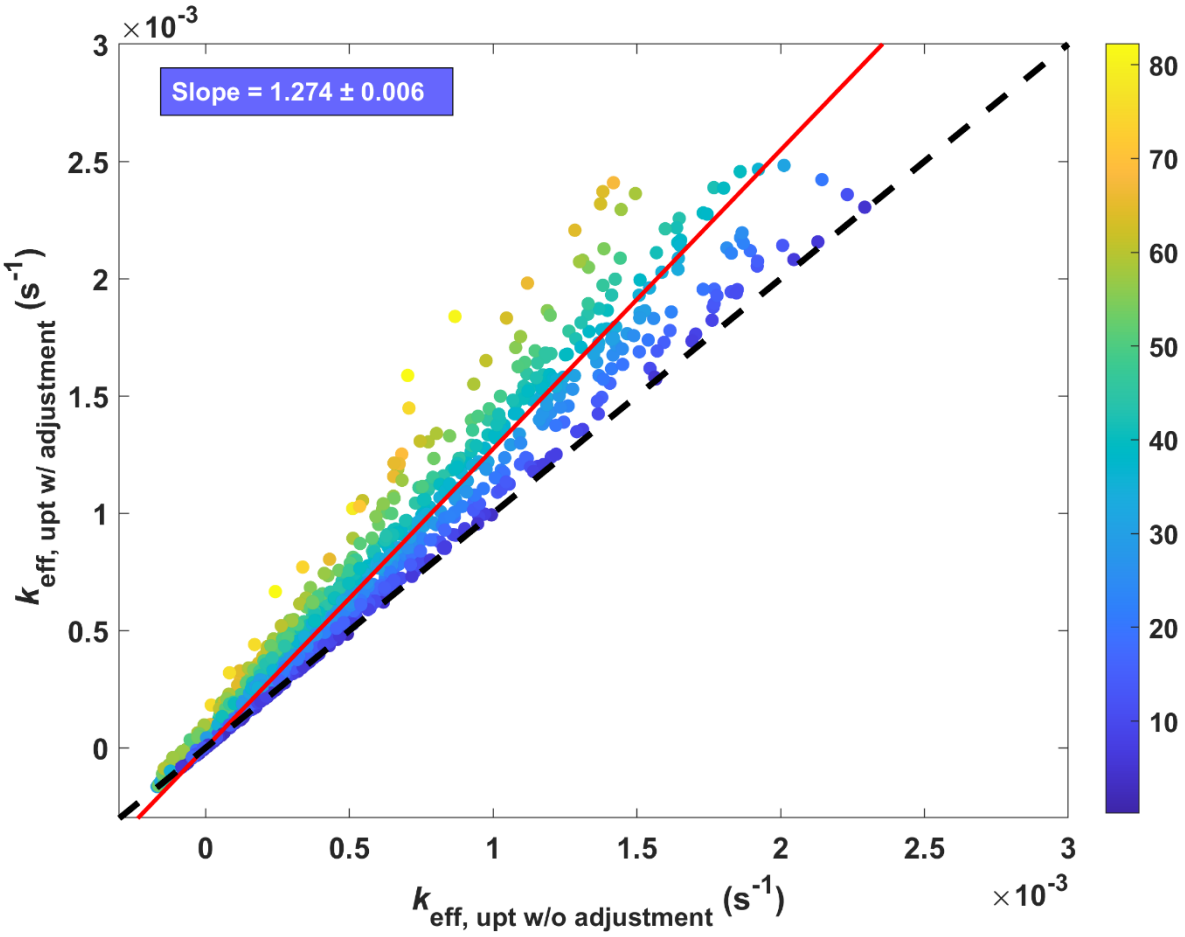

Figure S4. Comparison plot of effective aerosol uptake rate of CHOCHO ($k_{eff,uptake}$) with and without $Photo_{age}$ dependent adjustment. Black dashed line shows 1:1 line and red line is for ODR.

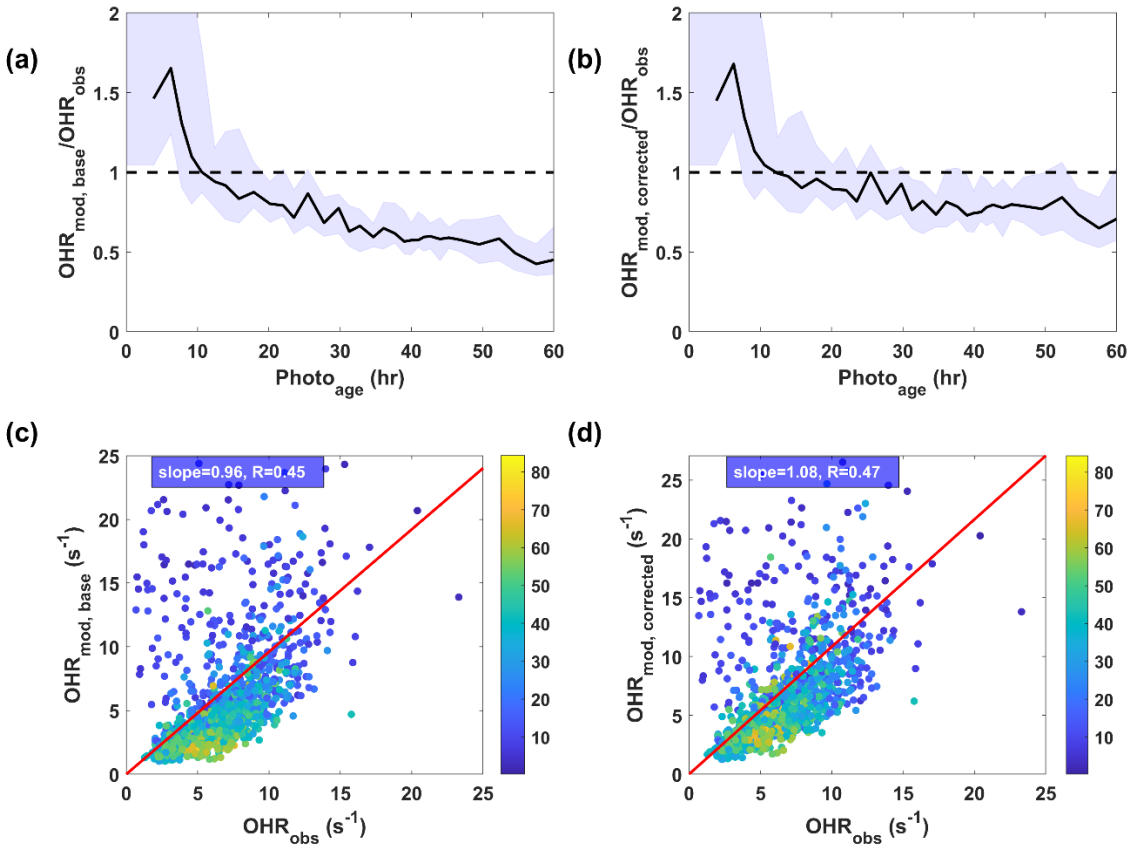

Figure S5. Same as Fig. S2 but OHR (OH reactivity) as a representative of oVOCs (oxygenated Volatile Organic Compounds)

80

S4. Aqueous phase treatment in the semi-explicit method.

Aqueous CHOCHO concentration, $[Gly]_{eq}$, including monomer, hydrates and oligomers, was treated as in equilibrium with gas-phase CHOCHO ($[Gly]_{obs}$) governed by effective Henry's law coefficient, K_{H,eff_gly} as Eq. (S1). CHOCHO contribution in SOA formation by OH oxidation in the aqueous phase in Knote et al. (2014) was replaced with effective photochemical reaction of glyoxal hydrates adopting rate coefficient, $k_{photochem}$ = 2 s^{-1}, from Ervens and Volkamer (2010), as aqueous OH concentration is highly uncertain. Here, $[Gly]_{mon+hyd,\ eq}$ refers to glyoxal monomer and its hydrates and we assume that the steady-state of $[Gly]_{mon+hyd,\ eq}$ is achieved with oligomers instantaneously as in right hand side of Eq. (S1), which is parameterized with oligomerization constant (K_{olig}), since $[Gly]_{mon+hyd,\ eq}$ lifetime is very short (0.5 sec). The time evolution of monomer and hydrates (Eq. S2) and eventually in steady-state, $[Gly]_{mon+hyd,\ SS}$), is determined as Eq. (S3). τ is the build-up time scale of $[Gly]_{mon+hyd}$ by the diffusion of gas phase CHOCHO, and laboratory study based values, 2.5×10^{2} s and 4.4×10^{5} s, are used for C_{AS} < 12 *m* and C_{AS} > 12 *m*, respectively, following Kampf et al. (2013). Then, the glySOA formation rate by the aqueous photochemical reaction of glyoxal, $P_{glySOA,\ eff.\ photochem}$, is analytically determined as Eq. (S4).

$$[Gly]_{eq}=K_{H,eff\_gly}\cdot[Gly]_{obs}=(K_{olig}+1)[Gly]_{mon+hyd,\ eq} \quad (S1)$$

$$\frac{d[Gly]_{mon+hyd}}{dt}=\frac{1}{\tau}\left([Gly]_{mon+hyd,\ eq}-[Gly]_{mon+hyd}\right)-k_{photochem}[Gly]_{mon+hyd}\approx 0 \quad (S2)$$

$$[Gly]_{mon+hyd,\ SS}=\left(\frac{\frac{1}{\tau}}{\frac{1}{\tau}+k_{photochem}}\right)\cdot[Gly]_{mon+hyd,\ eq} \quad (S3)$$

$$\frac{d[CHOCHO]_{vol,\ photochem}}{dt}=P_{glySOA,\ eff.\ photochem}\cong k_{photochem}[Gly]_{mon+hyd,\ SS}\cdot ALWC \quad (S4)$$

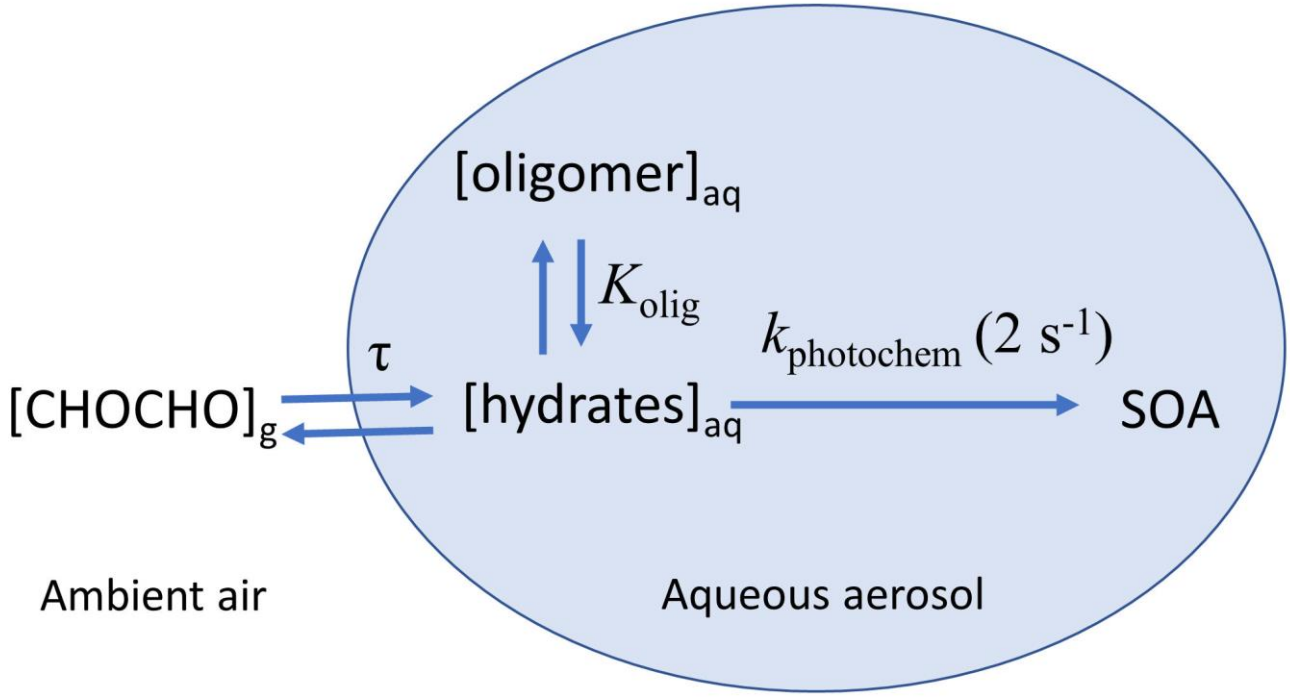

Figure S6. Schematic diagram of CHOCHO partitioning to aerosol liquid water and formation of SOA by effective photochemical reaction.

S5. Few representative VOCs distributions over Korean peninsula.

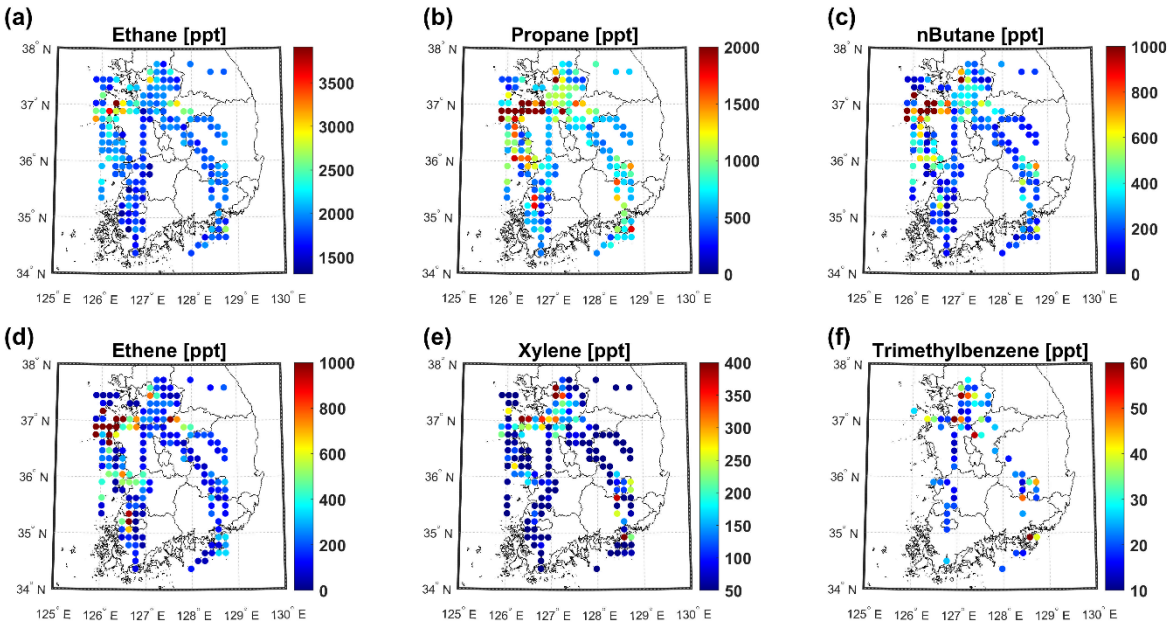

Figure S7. The geographically averaged (latitude: 0.14º, longitude: 0.15º and below 2 km altitude) few representative VOCs distributions; (a) ethane, (b) propane, (c) n-butane, (d) ethene, (d) xylene and (e) trimethylbenzene.

105

S6. Errors in effective uptake rate coefficient ($k_{eff,uptake}$) estimation.

In order to test the robustness of our modeled $k_{eff,uptake}$ against measurement uncertainties in VOCs measurements, varying VOCs concentrations of ±10 % were set as inputs for estimating $k_{eff,uptake}$, where the measurement errors were 5, 11 and 7 % for VOCs from WAS (Simpson et al. 2020), benzene and toluene from PTR-TOF-MS (Müller et al. 2014), respectively. Figure S8 shows the sensitivity of $k_{eff,uptake}$ with varying input concentrations of VOCs, resulting in ±10 % variation in $k_{eff,uptake}$ estimations.

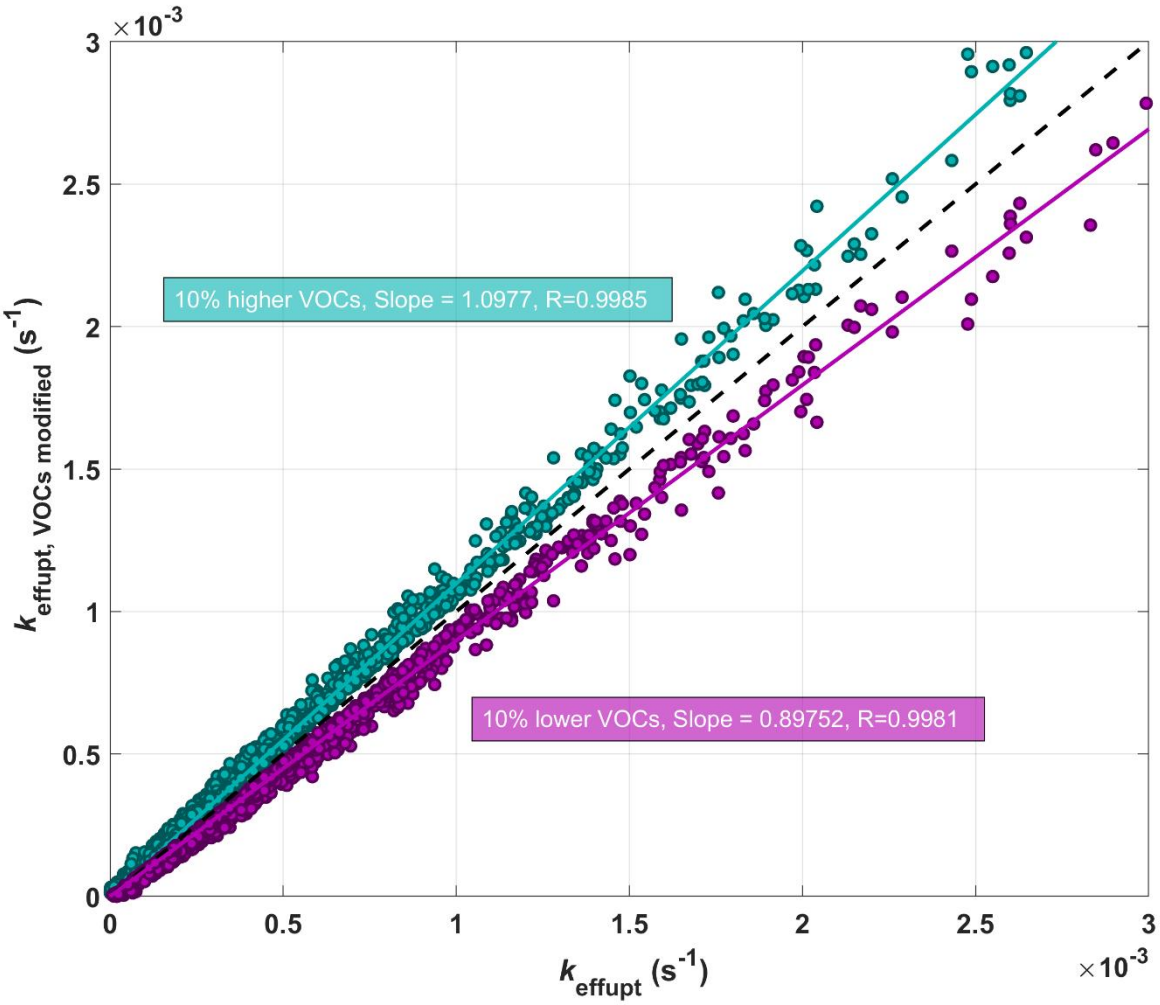

Figure S8. Effective uptake rate coefficient, $k_{eff,uptake}$, sensitivity test results with varying VOC input concentrations by ±10 %.

S7. Solar zenith angle and altitude dependent CHOCHO lifetime.

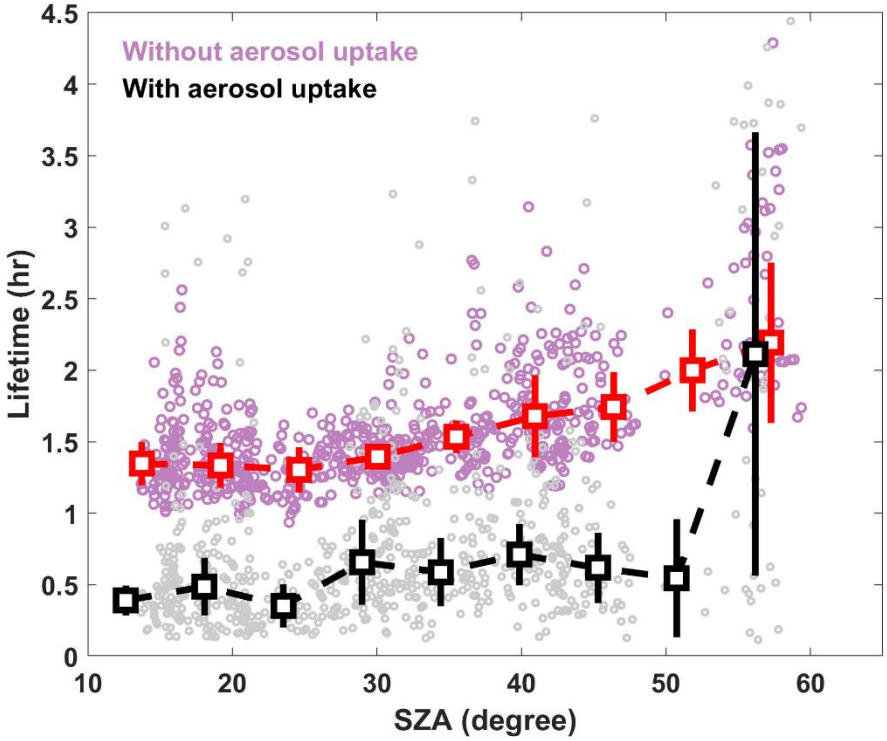

Figure S9. Lifetime of CHOCHO with respect to (a) solar zenith angle (SZA) with and without aerosol uptake (black and red, respectively).

S8. Aerosol volume distribution with respect to the aerosol surface area density change.

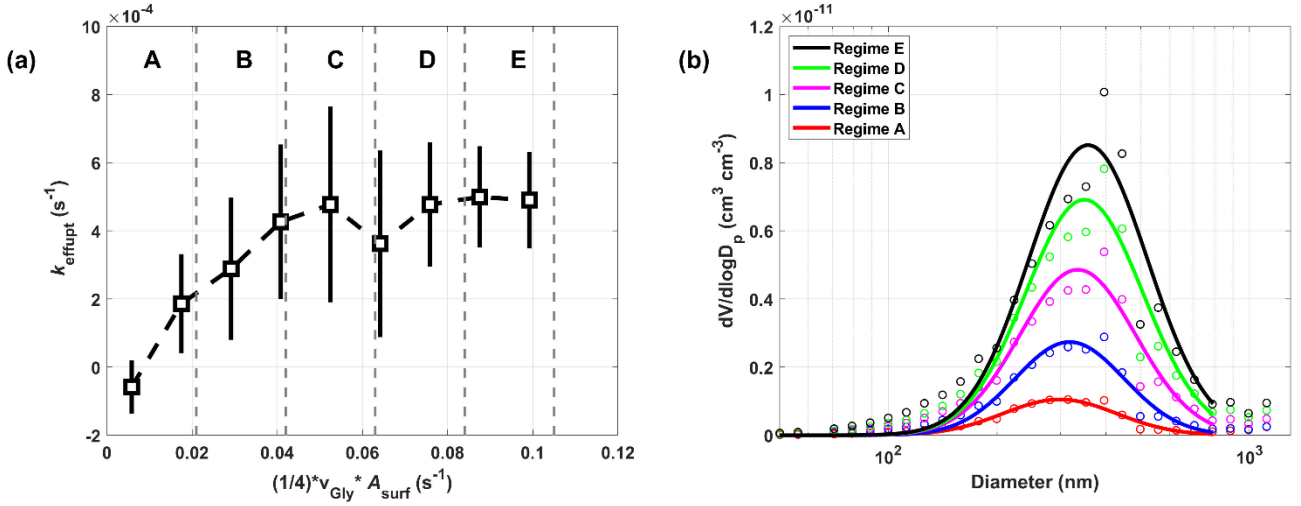

Figure S10. (a) The $k_{eff,uptake}$ dependence on aerosol surface area density (A_{surf}) scaled with (1/4)× v (mean molecular speed) with 5 equally divided regimes (mean ±1σ variability) and (b) averaged aerosol volume distribution at each A_{surf} regime (circles: average volume density, solid line: lognormal fit).

S9. 0-D box model and hybrid mechanism comparison for CHOCHO loss to aerosol.

We compared CHOCHO-induced SOA production rate from the 0-D box model and hybrid mechanism (Eq. S5) that includes aqueous-phase photochemistry ($P_{\text{glySOA, eff, photochem}}$, Eq. S6) with surface uptake ($P_{\text{glySOA, surface}}$, Eq. S7).

$$P_{\text{glySOA, hybrid}} = P_{\text{glySOA, eff, photochem}} + P_{\text{glySOA, surface}} \quad \text{(S5)}$$

$$P_{\text{glySOA, eff, photochem}} \cong k_{\text{photochem}}[\text{Gly}]_{\text{mon+hyd, SS}} \quad \text{(S6)}$$

$$P_{\text{glySOA, surface}} = k_{\text{surf,uptake}} \cdot [\text{CHOCHO}]_{\text{obs}} \quad \text{(S7)}$$

S9. Effective Henry's law coefficient in Regime I.

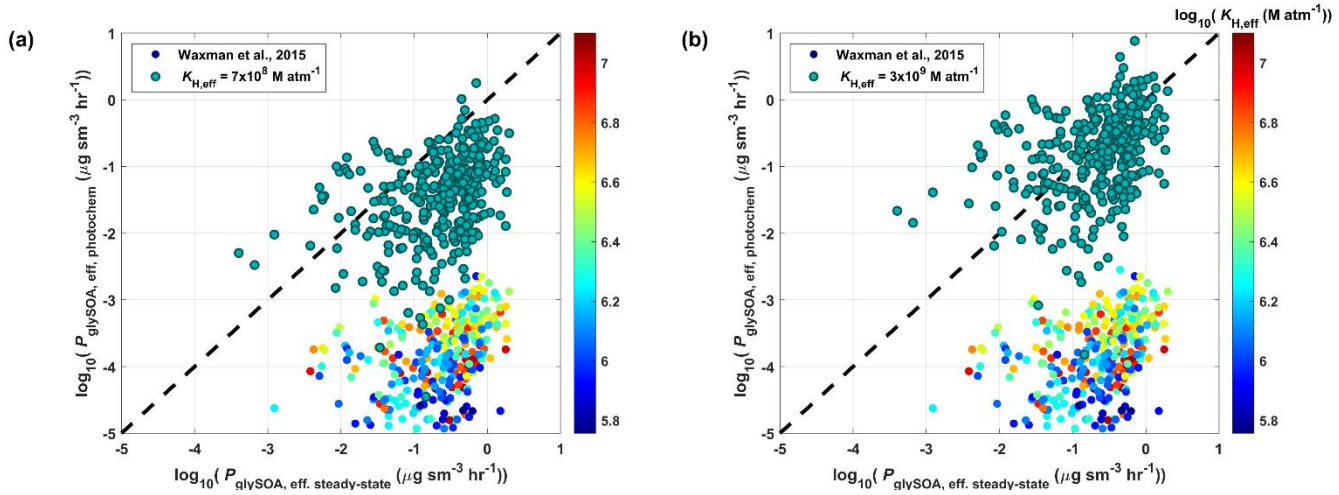

Figure S11. Comparison of glySOA production rate (P_{glySOA}) between steady-state and semi-explicit analysis for Regime I with one fixed Henry's law constant, $K_{\mathrm{H,eff\_Gly}}$ (green circles) of (a) 7.0×10^{8} M atm^{-1} which is an empirical value extracted from Regime II and (b) 3.0×10^{9} M atm^{-1} for the best agreement. The colored circles are calculated $K_{\mathrm{H,eff\_Gly}}$ based on inorganic salts concentrations by following Waxman et al. (2015).

S10. CHOCHO driven SOA formation for each research flight.

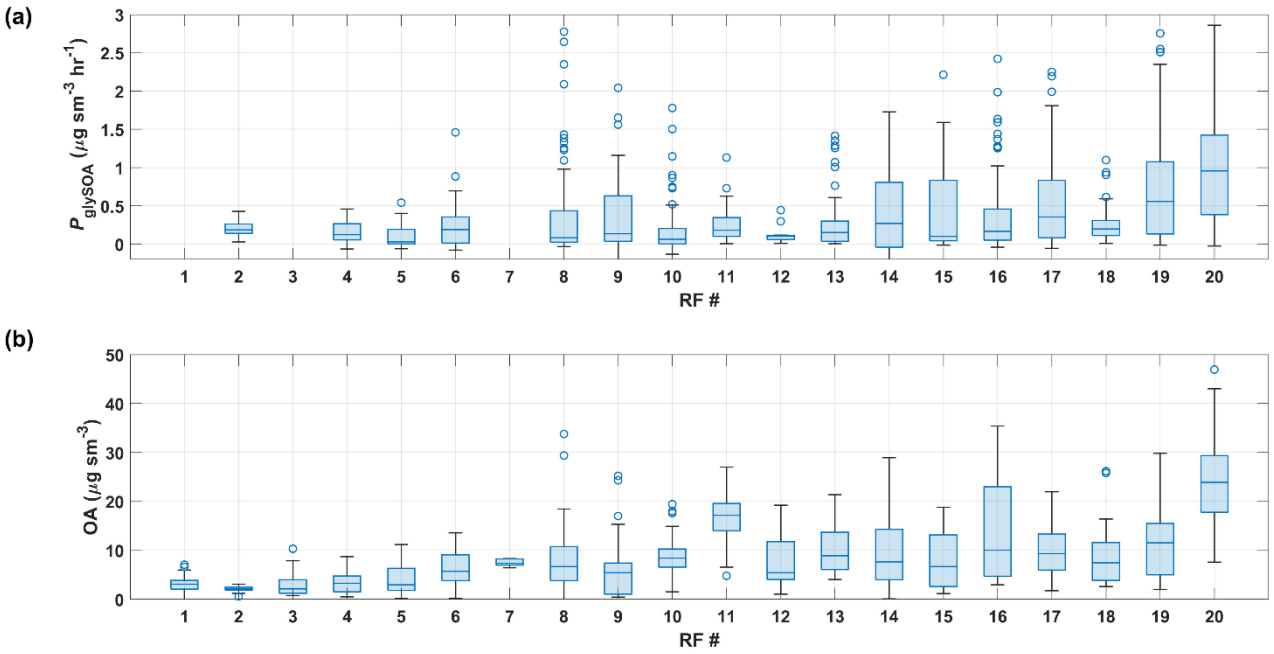

Figure S12. Box whisker plots of (a) CHOCHO induced SOA production rate and (b) OA mass loading for individual research flights (RF) over SMA (Seoul Metropolitan Area). Here, the box represents interquartile range, line inside the box is median, lower and upper whiskers are 10th and 90th percentiles, and circles are the data falling outside of 10th and 90th percentiles.

References

Brune, W. H., Miller, D. O., Thames, A. B., Allen, H. M., Apel, E. C., Blake, D. R., Bui, T. P., Commane, R., Crounse, J. D., Daube, B. C., Diskin, G. S., DiGangi, J. P., Elkins, J. W., Hall, S. R., Hanisco, T. F., Hannun, R. A., Hintsa, E. J., Hornbrook, R. S., Kim, M. J., McKain, K., Moore, F. L., Neuman, J. A., Nicely, J. M., Peischl, J., Ryerson, T. B., St. Clair, J. M., Sweeney, C., Teng, A. P., Thompson, C., Ullmann, K., Veres, P. R., Wennberg, P. O. and Wolfe, G. M.: Exploring oxidation in the remote free troposphere: Insights from atmospheric tomography (ATom), J. Geophys. Res., 125(1), doi:10.1029/2019jd031685, 2020.

DeCarlo, P. F., Ulbrich, I. M., Crounse, J., de Foy, B., Dunlea, E. J., Aiken, A. C., Knapp, D., Weinheimer, A. J., Campos, T., Wennberg, P. O. and Jimenez, J. L.: Investigation of the sources and processing of organic aerosol over the Central Mexican Plateau from aircraft measurements during MILAGRO, Atmos. Chem. Phys., 10(12), 5257–5280, doi:10.5194/acp-10-5257-2010, 2010.

Ervens, B. and Volkamer, R.: Glyoxal processing by aerosol multiphase chemistry: towards a kinetic modeling framework of secondary organic aerosol formation in aqueous particles, Atmos. Chem. Phys., 10(17), 8219–8244, doi:10.5194/acp-10-8219-2010, 2010.

Freney, E. J., Sellegri, K., Canonaco, F., Colomb, A., Borbon, A., Michoud, V., Doussin, J.-F., Crumeyrolle, S., Amarouche, N., Pichon, J.-M., Bourianne, T., Gomes, L., Prevot, A. S. H., Beekmann, M. and Schwarzenböeck, A.: Characterizing the impact of urban emissions on regional aerosol particles: airborne measurements during the MEGAPOLI experiment, Atmos. Chem. Phys., 14(3), 1397–1412, doi:10.5194/acp-14-1397-2014, 2014.

Hayes, P. L., Ortega, A. M., Cubison, M. J., Froyd, K. D., Zhao, Y., Cliff, S. S., Hu, W. W., Toohey, D. W., Flynn, J. H., Lefer, B. L., Grossberg, N., Alvarez, S., Rappenglück, B., Taylor, J. W., Allan, J. D., Holloway, J. S., Gilman, J. B., Kuster, W. C., de Gouw, J. A., Massoli, P., Zhang, X., Liu, J., Weber, R. J., Corrigan, A. L., Russell, L. M., Isaacman, G., Worton, D. R., Kreisberg, N. M., Goldstein, A. H., Thalman, R., Waxman, E. M., Volkamer, R., Lin, Y. H., Surratt, J. D., Kleindienst, T. E., Offenberg, J. H., Dusanter, S., Griffith, S., Stevens, P. S., Brioude, J., Angevine, W. M. and Jimenez, J. L.: Organic aerosol composition and sources in Pasadena, California, during the 2010 CalNex campaign, J. Geophys. Res., 118(16), 9233–9257, doi:10.1002/jgrd.50530, 2013.

Hu, W., Hu, M., Hu, W., Jimenez, J. L., Yuan, B., Chen, W., Wang, M., Wu, Y., Chen, C., Wang, Z., Peng, J., Zeng, L. and Shao, M.: Chemical composition, sources, and aging process of submicron aerosols in Beijing: Contrast between summer and winter, J. Geophys. Res., 121(4), 1955–1977, doi:10.1002/2015jd024020, 2016.

Kampf, C. J., Waxman, E. M., Slowik, J. G., Dommen, J., Pfaffenberger, L., Praplan, A. P., Prévôt, A. S. H., Baltensperger, U., Hoffmann, T. and Volkamer, R.: Effective Henry's law partitioning and the salting constant of glyoxal in aerosols containing sulfate, Environ. Sci. Technol., 47(9), 4236–4244, doi:10.1021/es400083d, 2013.

Knote, C., Hodzic, A., Jimenez, J. L., Volkamer, R., Orlando, J. J., Baidar, S., Brioude, J., Fast, J., Gentner, D. R., Goldstein, A. H., Hayes, P. L., Knighton, W. B., Oetjen, H., Setyan, A., Stark, H., Thalman, R., Tyndall, G., Washenfelder, R., Waxman, E. and Zhang, Q.: Simulation of semi-explicit mechanisms of SOA formation from glyoxal in aerosol in a 3-D model, Atmos. Chem. Phys., 14(12), 6213–6239, doi:10.5194/acp-14-6213-2014, 2014.

Ma, P. K., Zhao, Y., Robinson, A. L., Worton, D. R., Goldstein, A. H., Ortega, A. M., Jimenez, J. L., Zotter, P., Prévôt, A. S. H., Szidat, S. and Hayes, P. L.: Evaluating the impact of new observational constraints on P-S/IVOC emissions, multi-generation oxidation, and chamber wall losses on SOA modeling for Los Angeles, CA, Atmos. Chem. Phys., 17(15), 9237–9259, doi:10.5194/acp-17-9237-2017, 2017.

Marvin, M. R., Wolfe, G. M., Salawitch, R. J., Canty, T. P., Roberts, S. J., Travis, K. R., Aikin, K. C., de Gouw, J. A., Graus, M., Hanisco, T. F., Holloway, J. S., Hübler, G., Kaiser, J., Keutsch, F. N., Peischl, J., Pollack, I. B., Roberts, J. M., Ryerson, T. B., Veres, P. R. and Warneke, C.: Impact of evolving isoprene mechanisms on simulated formaldehyde: An inter-

comparison supported by in situ observations from SENEX, Atmos. Environ., 164, 325–336, doi:10.1016/j.atmosenv.2017.05.049, 2017.

Müller, M., Mikoviny, T., Feil, S., Haidacher, S., Hanel, G., Hartungen, E., Jordan, A., Märk, L., Mutschlechner, P., Schottkowsky, R., Sulzer, P., Crawford, J. H. and Wisthaler, A.: A compact PTR-ToF-MS instrument for airborne measurements of volatile organic compounds at high spatiotemporal resolution, Atmos. Meas. Tech., 7(11), 3763–3772, doi:10.5194/amt-7-3763-2014, 2014.

Nault, B. A., Campuzano-Jost, P., Day, D. A., Schroder, J. C., Anderson, B., Beyersdorf, A. J., Blake, D. R., Brune, W. H., Choi, Y., Corr, C. A., de Gouw, J. A., Dibb, J., DiGangi, J. P., Diskin, G. S., Fried, A., Huey, L. G., Kim, M. J., Knote, C. J., Lamb, K. D., Lee, T., Park, T., Pusede, S. E., Scheuer, E., Thornhill, K. L., Woo, J.-H. and Jimenez, J. L.: Secondary organic aerosol production from local emissions dominates the organic aerosol budget over Seoul, South Korea, during KORUS-AQ, Atmos. Chem. Phys., 18(24), 17769–17800, doi:10.5194/acp-18-17769-2018, 2018.

Ortega, A. M., Hayes, P. L., Peng, Z., Palm, B. B., Hu, W., Day, D. A., Li, R., Cubison, M. J., Brune, W. H., Graus, M., Warneke, C., Gilman, J. B., Kuster, W. C., de Gouw, J., Gutiérrez-Montes, C. and Jimenez, J. L.: Real-time measurements of secondary organic aerosol formation and aging from ambient air in an oxidation flow reactor in the Los Angeles area, Atmos. Chem. Phys., 16(11), 7411–7433, doi:10.5194/acp-16-7411-2016, 2016.

Schroeder, J. R., Crawford, J. H., Ahn, J.-Y., Chang, L., Fried, A., Walega, J., Weinheimer, A., Montzka, D. D., Hall, S. R., Ullmann, K., Wisthaler, A., Mikoviny, T., Chen, G., Blake, D. R., Blake, N. J., Hughes, S. C., Meinardi, S., Diskin, G., Digangi, J. P., Choi, Y., Pusede, S. E., Huey, G. L., Tanner, D. J., Kim, M. and Wennberg, P.: Observation-based modeling of ozone chemistry in the Seoul metropolitan area during the Korea-United States Air Quality Study (KORUS-AQ), Elementa (Wash., DC), 8(1), 3, doi:10.1525/elementa.400, 2020.

Simpson, I. J., Blake, D. R., Blake, N. J., Meinardi, S., Barletta, B., Hughes, S. C., Fleming, L. T., Crawford, J. H., Diskin, G. S., Emmons, L. K., Fried, A., Guo, H., Peterson, D. A., Wisthaler, A., Woo, J.-H., Barré, J., Gaubert, B., Kim, J., Kim, M. J., Kim, Y., Knote, C., Mikoviny, T., Pusede, S. E., Schroeder, J. R., Wang, Y., Wennberg, P. O. and Zeng, L.: Characterization, sources and reactivity of volatile organic compounds (VOCs) in Seoul and surrounding regions during KORUS-AQ, Elementa (Wash., DC), 8(1), 37, doi:10.1525/elementa.434, 2020.

Waxman, E. M., Elm, J., Kurtén, T., Mikkelsen, K. V., Ziemann, P. J. and Volkamer, R.: Glyoxal and Methylglyoxal Setschenow Salting Constants in Sulfate, Nitrate, and Chloride Solutions: Measurements and Gibbs Energies, Environ. Sci. Technol., 49(19), 11500–11508, doi:10.1021/acs.est.5b02782, 2015.